International Journal of Heat and Technology
Vol. 42, No. 4, August, 2024, pp. 1337-1348
Journal homepage: http://iieta.org/journals/ijht

Numerical Investigation of Material and Structural Influence on Transient Temperature Behavior in Disc Brakes During Single-Stop Braking

Chau Nguyen Minh[1*], Quan Do Van[1], Tan Nguyen Dinh[2], Quynh Le Van[1]

[1] Faculty of Automotive and Power Machinery Engineering, Thai Nguyen University of Technology, Thai Nguyen 250000, Viet Nam
[2] Faculty of Mechanical Engineering, East Asia University of Technology, Bac Ninh 790000, Viet Nam

Corresponding Author Email: minhchau-ice@tnut.edu.vn

https://doi.org/10.18280/ijht.420424

Received: 22 May 2024
Revised: 12 July 2024
Accepted: 1 August 2024
Available online: 31 August 2024

Keywords:
disc brake, solid disc brake, ventilated disc brake, transient temperature field, finite element method (FEM)

ABSTRACT

While many techniques have been proposed to enhance heat dissipation in ventilated disc brakes during extended braking, solid disc brakes have received less attention, particularly under hard braking conditions. This study investigates the transient thermal responses of both solid and ventilated disc brakes during single-stop braking. Numerical simulations were conducted on three disc types: Solid, ventilated with 32 fins, and ventilated with 42 fins, each made from different materials: Grey cast iron, AISI 420, and INCONEL 718. The simulations assessed the maximum surface temperature and the temperature distribution across the disc thickness. The results indicate significant differences in thermal performance based on material properties and disc design. Grey cast iron exhibited the lowest maximum temperatures due to its high thermal conductivity, whereas INCONEL 718 showed the highest temperatures due to its lower thermal conductivity. Despite their improved cooling capabilities, ventilated discs demonstrated higher maximum surface temperatures compared to solid discs, due to their lower thermal capacity. These findings highlight the importance of material selection and structural design in optimizing brake disc performance under high thermal loads.

1. INTRODUCTION

The braking system is a vehicle component responsible for decelerating it to a lower speed or bringing it to a complete stop. It operates by applying friction, converting kinetic energy into heat, which raises the temperature of the system's components [1]. The primary components of a disc braking system include the disc rotor, brake pads, and calipers [2, 3]. The disc is bolted to the wheel hub, rotating with the wheel. Attached to the steering knuckle, the caliper holds the pads and presses them against the disc. During braking events, fluid pressure forces the pads against both sides of the disc, generating heat. Most of this heat, around 90%, is absorbed by the disc rotor through conduction [4, 5]. The heat is then dissipated to the surrounding air through convection heat transfer [4, 6, 7]. The rapid temperature rise in the brake disc and pads reduces braking performance and causes thermal wear [8, 9], brake fade [10], and thermal cracking [11].

Rhee [10] concluded that decreasing the coefficient of friction from 0.4 to 0.3 could reduce the brake torque by up to 25%. Duzgun [12] studied the thermal characteristics of ventilated brake discs during continuous braking. His findings showed that using ventilation can lower the temperature of solid brake disc surfaces by as much as 24%. Mackin et al. [11] discussed the thermal cracking of disc brakes and concluded that this problem can be solved in three ways: Selecting the optimal material for the disc rotor, lowering the disc's temperature, and redesigning the hub-rotor unit. In order to reduce the impact of temperature on braking performance, various studies on the complex phenomenon of heat dissipation in the disc and pads have been conducted over the years.

Limpert [13] evaluated the cooling efficiency of solid versus ventilated discs and showed that the internal ventilation of the ventilated disc brake becomes significant only when the rotor speed exceeds a critical value. Coulibaly et al. [14] numerically studied the use of thermoelectric generators in vehicles to convert heat into electrical energy during the braking process. They showed that using a ventilated disc brake instead of a solid disc brake reduced the disc's maximum surface temperature from 222°C to 175°C. Jafari and Akyüz [15] conducted numerical research on improving the design of ventilated disc brakes to enhance cooling performance. Their findings indicated that the width of the ventilation gap was the most significant factor. Li and Yang [16] investigated the optimization of ventilated disc geometry to enhance cooling performance. Their results showed that increasing the ventilation gap and the bending angle of the cooling fins can improve the cooling effect. All the mentioned studies have demonstrated the effect of ventilated discs on cooling performance during extended braking, such as when a vehicle descends a hill. However, research comparing the temperatures of solid and ventilated disc brakes under hard braking conditions (a single stop where the vehicle is brought

to a complete stop from high speed) appears to be lacking. Furthermore, it has been discovered that solid disc brakes offer lower aerodynamic losses compared to ventilated disc brakes [17].

This paper aims to investigate the thermal behavior of solid and ventilated disc brakes during single-stop braking. Numerical simulations were performed for three types of discs (solid disc, ventilated disc with 32 fins, and ventilated disc with 42 fins) made of different materials (grey cast iron, AISI 420, INCONEL 718). A comparison among the three disc configurations was conducted based on the maximum temperature on the surface and the temperature distribution across the disc thickness.

This paper is organized as follows: Section 2 introduces the theory behind disc brake heat flux during braking. Section 3 describes the brake disc model's geometry and the simulation methodology employed. In Section 4, we present and analyze the numerical results. Model validation is covered in Section 4.1, featuring comparisons with existing models. Section 4.2 investigates the effects of material properties on the disc brake's transient temperature profiles, while Section 4.3 analyzes how structural variations influence these temperature distributions. Section 5 concludes with final remarks.

2. THEORY OF DISC BRAKE HEAT FLUX

This section briefly represents the history of heat flux in the disc brake. The heat flux is considered the frictional heat input load between the brake disc and the pad, which is applied to the friction surface of the brake disc during the simulation process. The following assumptions are made before calculating: The material properties of the brake disc are isotropic and independent of temperature. The brake pad pressure remains constant during the braking process. The friction coefficient between the brake disc and the pad is constant during braking. The convective heat transfer coefficient of the brake disc surface is constant. Radiation heat transfer is neglected due to the short braking time and low temperature. All kinetic energy at the disc brake surface is converted into frictional heat, which is uniformly distributed to the surface of the brake disc through heat flux.

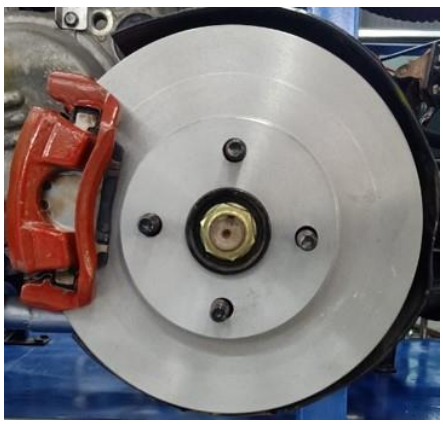

Figure 1. Disk brake assembly with a rotor and a caliper

Figure 1 illustrates a typical automotive disc brake, which includes a disc rotor and a caliper. The caliper holds two pads and presses them against both sides of the disc rotor. Each brake pad consists of a steel backing plate with friction material bonded to its surface. During braking, the friction material on both pads contacts the disc rotor, generating friction that slows down or stops the vehicle. The sliding contact model of the friction pair is depicted in Figure 2.

During braking, the pads are forced onto both sides of the disc, generating heat in this action. Two models have been proposed to calculate the heat generation in this process: the Macroscopic model and the Microscopic model [18]. This study uses the Microscopic model. The following is a brief overview of this method.

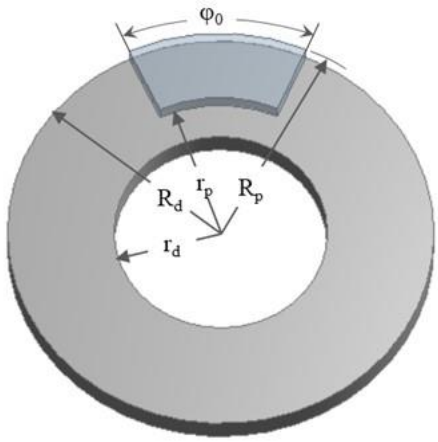

Figure 2. A schematic contact model of the pad-disc braking system

The quantity of heat generated in the contact zone between the disc and pad is directly proportional to the friction force. When the brake pads press against the rotating disc, friction between the surfaces converts kinetic energy into thermal energy. This heat is absorbed by the disc, which accounts for approximately 90% of the heat [4, 5], and by the pads and other components of the brake system. Two models have been proposed to describe thermal contact: The perfect contact and the imperfect contact models [19]. This study uses the imperfect contact model. In this model, a third body of detached particles is introduced between the disc and pad surfaces. When employing this model, the heat flux on the disc and pad is calculated as following [18].

First, the thermal effusivity of the disc (ξ_d) and thermal effusivity of the pad (ξ_p) were defined as:

$$\xi_d = \sqrt{k_d \rho_d c_d} \tag{1}$$

$$\xi_p = \sqrt{k_p \rho_p c_p} \tag{2}$$

where, the subscripts d and p denote the disc and the pad, respectively; k represents thermal conductivity; ρ denotes density; and c stands for specific heat.

The contact surfaces area of the disc (S_d) and pad (S_p) are determined using the following equations:

$$S_d = 2\pi \int_{r_d}^{R_d} r dr \tag{3}$$

$$S_p = \varphi_0 \int_{r_p}^{R_p} r dr \tag{4}$$

Second, the coefficient of heat partition is calculated using Eq. (5) [20]:

$$\gamma = \frac{\xi_d S_d}{\xi_d S_d + \xi_p S_p} \tag{5}$$

As previously mentioned, we assumed that all friction power is converted into thermal energy. Consequently, the heat generation rate resulting from friction between the contact zones of the disc and pad surfaces is computed using the following equations:

$$d\dot{E} = dP_{br} = VdF_f = r\omega\mu p\varphi_0 r dr \tag{6}$$

$$d\dot{E} = d\dot{E}_p + d\dot{E}_d \tag{7}$$

$$d\dot{E}_p = (1-\gamma)dP_{br} = (1-\gamma)\mu p\omega\varphi_0 r^2 dr \tag{8}$$

$$d\dot{E}_d = \gamma dP_{br} = \gamma\mu p\omega\varphi_0 r^2 dr \tag{9}$$

where, $d\dot{E}$ is the rate of heat generated at the contact zone of disc-pad, P_{br} is the brake power, V is the relative sliding velocity ($V = r.\omega$) and dF_f is the friction force, $dF_f = \mu dF_n = \mu p dA$ (Figure 3), where F_n is the normal force and μ is the coefficient of friction [3, 21]. $d\dot{E}_p$ and $d\dot{E}_d$ are the heat absorbed by the pad and disc, respectively. Furthermore, this work assumes that the vehicle's velocity decelerates at a constant rate during the braking process. Therefore, the wheel speed can be determined in Eq. (10):

$$\omega(t) = \omega_0\left(1 - \frac{t}{t_b}\right) \tag{10}$$

where, t_b is the braking time.

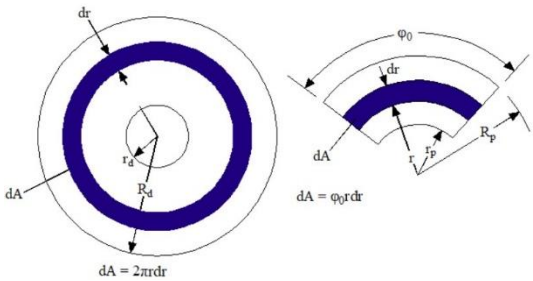

(a) (b)

Figure 3. Components of the contact surface element - (a) the disk, and (b) the pad

Then, the heat flux to the pad surface $q_1(r,t)$ and to the disc surface $q_2(r,t)$ were calculated by dividing $d\dot{E}_p$ and $d\dot{E}_d$ by dS_p and dS_d, respectively.

$$q_1(r,t) = \frac{d\dot{E}_p}{dS_p} = (1-\gamma)\mu pr\omega(t) \tag{11}$$

$$q_2(r,t) = \frac{d\dot{E}_d}{dS_d} = \frac{\varphi_0}{2\pi}\gamma\mu pr\omega(t) \tag{12}$$

The pressure distributions have been suggested in two models: Uniform pressure and uniform wear. This study used for the second one. Hence, the pressure distribution can be expressed using following equation:

$$p = p_{max}\frac{r_p}{r} \tag{13}$$

where, p_{max} represents the peak pressure distributed across the pad, p is pressure at radial position r, and r_p is the inner radius in pad (Figure 3). When entered $p = p_{max}\frac{r_p}{r}$ and ω(t) into Eq. (13), the result of heat flux on the disc is:

$$q_2(t) = \frac{d\dot{E}_d}{dS_d} = \frac{\varphi_0}{2\pi}\gamma\mu p_{max} r_p \omega_0\left(1 - \frac{t}{t_b}\right) \tag{14}$$

3. MATERIALS AND METHODS

3.1 Geometry

This paper analyzes three types of disc geometries based on a light vehicle: (1) a solid disc, (2) a ventilated disc with 32 straight fins, and (3) a ventilated disc with 42 straight fins. The models were created using the ANSYS Workbench platform. Figure 4 illustrates the dimensions and specifications of these discs, while Table 1 provides detailed material properties.

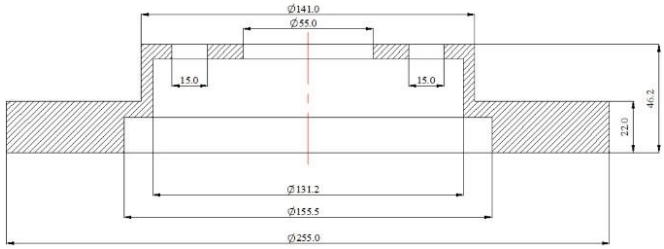

(a) Dimension of solid disc brake

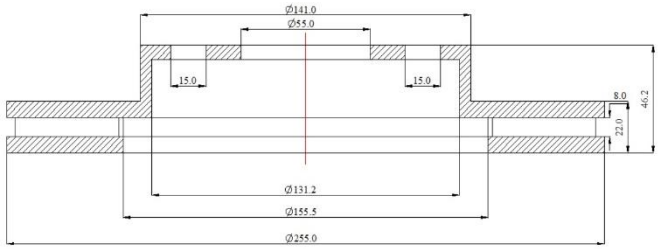

(b) Dimension of ventilated disc brake

(c) Three dimensional solid-type disc brake

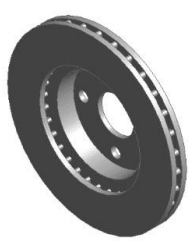

(d) Three-dimensional ventilated-type disc brake with 32 straight fins

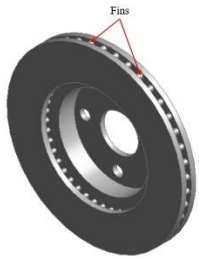

(e) Three-dimensional ventilated-type disc brake with 42 straight fins

Figure 4. Geometry of disc brake

Table 1. The values of the material properties

Material Properties	Grey Cast Iron	Inconel 718	AISI 420
Density (kg.m^{-3})	7850	8220	7800
Young's modulus (Gpa)	98	200	200
Poisson's ratio	0.27	0.29	0.28
Thermal expansion coefficient (μK^{-1})	11	13	11
Thermal conductivity (W.m^{-1}.K^{-1})	50	11	16
Specific heat capacity (J/K^{-1}.kg^{-1})	500	435	460

Note: Grey cast iron [22], and the materials are made with a nickel-based alloy type Inconel 718 [23], and martensitic stainless steel type AISI 420 [24].

Table 2. Mesh parameters

Mesh Parameters	
Method	MultiZone
Number of cells	106200
Number of nodes	507627
Maximum of skewness	3.285×10^{-3}
Minimum of skewness	0.70
Maximum Aspect Ratio	2.837
Minimum Aspect Ratio	1.014

3.2 Meshing

In this study, structured hexahedral mesh elements are used for the simulation, ensuring the creation of a mesh that is highly effective. These elements play a crucial role in enhancing both the speed and accuracy of the simulation [25, 26].

Mesh quality control is implemented to evaluate the final mesh's quality, employing the skewness method. This technique compares the shape of each mesh cell to that of an equilateral cell with an equivalent volume. Figure 5 and Table 2 provide an in-depth look at the mesh configuration and the criteria used for its formation. From Table 2, it is evident that the maximum skewness is 0.70, which falls within the 'good' category. Additionally, the table displays the maximum and minimum aspect ratios.

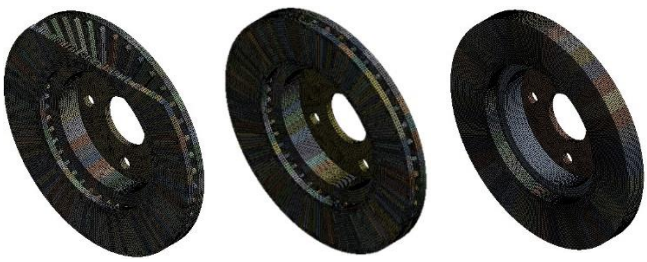

Figure 5. Mesh of the disc brake

3.3 Equations

The transient heat conduction equation of the disc brake can be described in the Cartesian coordinate system as follows [27-29]:

$$\rho c\left(\frac{\partial T_d}{\partial t}\right) = k\left\{\frac{\partial}{\partial x}\left(\frac{\partial T_d}{\partial x}\right) + \frac{\partial}{\partial y}\left(\frac{\partial T_d}{\partial y}\right) + \frac{\partial}{\partial z}\left(\frac{\partial T_d}{\partial z}\right)\right\} \quad (15)$$

The boundary conditions and initial condition can be specified as:

$$T_d = T^* \quad (16)$$

$$k_d\left\{\frac{\partial T_d}{\partial x}n_x + \frac{\partial T_d}{\partial y}n_y + \frac{\partial T_d}{\partial z}n_z\right\} = q_2(t) \quad (17)$$

$$k_d\left\{\frac{\partial T_d}{\partial x}n_x + \frac{\partial T_d}{\partial y}n_y + \frac{\partial T_d}{\partial z}n_z\right\} = -h(T_d - T_\infty) \quad (18)$$

$$T_d = T_0 = T_\infty \; at \; t = 0 \quad (19)$$

where, T^* is the specified surface temperature, h is the coefficient of convective heat transfer, T_0 is the initial temperature, T_∞ is the environmental temperature, and n_x, n_y, n_z are the normal unit vectors respectively.

3.4 Boundary conditions

In this study, the initial temperature throughout the entire model is 22℃ at time t = 0 seconds. This study lasts for four seconds, taking hard braking into account. The convective heat transfer coefficient (denoted as h) for heat transfer by convection is set up at 230Wm^{-2}.℃$^{-1}$. The model relies solely on the heat flux generated when the pads make contact with both sides of the disc during braking. This heat flux, denoted as $q_2(t)$, is calculated using Eq. (14). Its magnitude varies depending on the disc materials and braking time, as detailed in Table 3. It is also worth noting that the pad material used in this study is derived from the simulation [30].

Table 3. The values of the parameters used in numerical simulations

Parameter	Material		
	Grey Cast Iron	Inconel 718	AISI 420
Friction coefficient, μ	0.4		
Inner radius in disc, r_d (mm)	77.75		
Outer radius in disc, R_d (mm)	127.5		
Inner radius in pad, r_p (mm)	84.75		
Outer radius in pad, R_p (mm)	127.5		
Arc angle pad, φ_0 (deg)	65		
Pad fiction contact surface, S_p (m^2)	0.005147		
Disc fiction contact surface, S_d (m^2)	0.032079		
Initial angular velocity ω_0 (rad/s)	152.44		
Pressure p (Mpa)	1.3		
Braking time t_b (s)	4		
Thermal effusivity (Ws$^{1/2}$m^{2}K)	14008.93	6271.58	7576.81
Heat partition coefficient	0.97	0.94	0.95
Heat flux ($q_2(t)$)	$1.1773*10^6$ (1-t/4)	$1.1361*10^6$(1-t/4)	$1.1486*10^6$(1-t/4)

3.5 Grid independent test

Three-dimensional physical models of discs are employed for all computational models in this study. To assess mesh independence, three mesh sizes are examined: 50,926, 106,200, and 196,491 elements, with the mesh density nearly doubling with each refinement. Figure 6 illustrates the findings of the grid independence study, depicting the maximum temperature over time for various numbers of elements. The second size (106,200 elements) is utilized in the simulation.

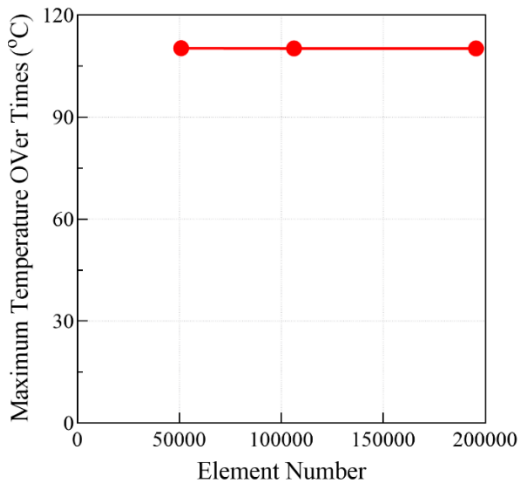

Figure 6. Grid independency test

4. RESULTS AND DISCUSSION

4.1 Comparison with existing studies

This section aims to validate the developed finite element model by comparing its calculations with existing literature. For this purpose, we used a current numerical method to reproduce the results of Dubale et al. [30].

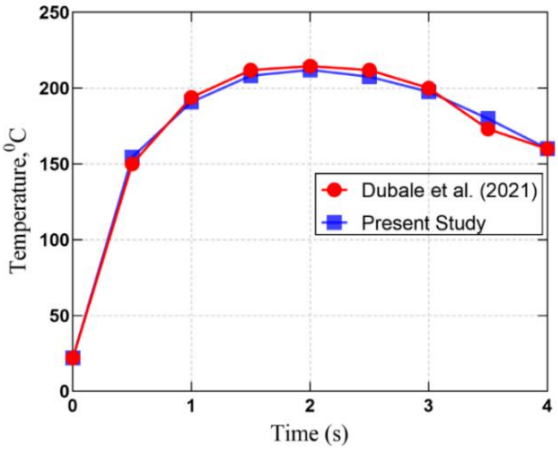

Note: Temperature trends over time from [30] (red solid line with circular dots) and current study (blue solid line with square dots)

Figure 7. Verification of temperature

Figure 7 illustrates the relationship between maximum temperature and time, showing a significant agreement between the results obtained from the numerical method in this work and previously published numerical results.

4.2 The influence of materials on disc brake transient temperature profiles

This section investigates the thermal characteristics of three disc models, with each model being fabricated from three different materials: GCI, Inconel 718, and AISI 420.

The ANSYS transient thermal model was employed to determine the maximum temperature over time and the temperature distribution contours. Figure 8 illustrates the maximum temperatures for three disc models, each made from different materials. These results are consistent with existing literature [31, 32]. As expected, differences in material properties lead to significant variations in thermal behaviour. The thermal conductivity of GCI (k_{GCI} = 50 W.m^{-1}. K^{-1})) is more than three times higher than that of AISI 420 ($K_{AISI\ 420}$ = 16 W.m^{-1}. K^{-1}) and over 4.5 times higher than that of Inconel 718 ($K_{Inconel\ 718}$ = 11 W.m^{-1}. K^{-1}). Consequently, the Inconel 718 disc brake reaches the highest maximum temperature over time, while the GCI disc brake has the lowest maximum temperature. The lower thermal conductivity of Inconel 718 limits heat dispersion, resulting in higher thermal energy retention compared to the GCI disc brake. Furthermore, the maximum temperature observed in these results is affected by the mass and specific heat capacity of the material used to fabricate the disc, as indicated in Eq. (20):

$$Q = mc_p\Delta T \tag{20}$$

where, Q(J) is amount of heat absorbed by the disc, m (kg) is the mass of disc, c_P (J.kg^{-1}) is the specific heat capacity of the material used to make the disc and ΔT is the temperature variation.

As illustrated in Table 3, the heat rates supplied to GCI, AISI 420, and Inconel 718 differ due to differences in the heat partition coefficient. Nonetheless, they can be considered equivalent for comparative purposes. Consequently, by setting Eq. (20) equal to GCI, AISI 420, and Inconel 718, the following relationships are obtained:

$$mc_p\Delta T|_{GCI} = mc_p\Delta T|_{AISI\ 420} = mc_p\Delta T|_{Inconel\ 718} \tag{21}$$

$$\frac{mc_p|_{GCI}}{mc_p|_{AISI420}} = \frac{\Delta T|_{AISI420}}{\Delta T|_{GCI}} \tag{22}$$

$$\frac{mc_p|_{AISI420}}{mc_p|_{Inconel718}} = \frac{\Delta T|_{Inconel718}}{\Delta T|_{AISI420}} \tag{23}$$

Substitute the values of mass of disc (note that m = ρV, where ρ is the density of body and V is the volume of body) and c_p from the Table 1 into these equations, we can draw the following relationship as below:

$$\rho Vc_p|_{Inconel718} < \rho Vc_p|_{AISI420} < \rho Vc_p|_{GCI} \tag{24}$$

$$\Delta T_{GCI} < \Delta T_{AISI420} < \Delta T_{Inconel718} \tag{25}$$

It can thus be observed that the results from Figure 8 follow this relationship successfully.

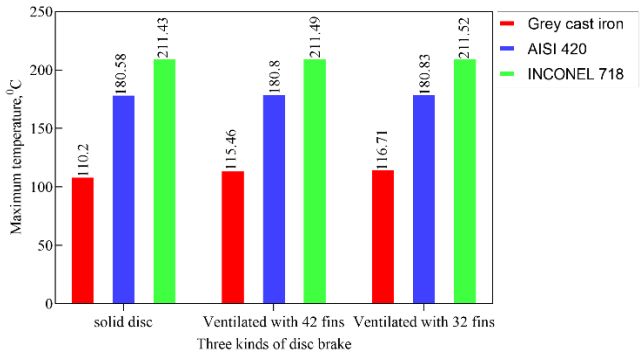

Figure 8. Maximum temperature of three disc models made from different materials: Gray cast iron (abbreviated as GCI), Inconel 718, and AISI 420

4.3 The influence of structure on disc brake transient temperature distributions

The simulation results of the thermal performance of three kinds of discs with the same material, grey cast iron, are presented in this section. In general, the heat of disk brake is dissipated by radiation, conduction, and convection. In this work, radiation is neglected, as in many other studies in the literature [3, 13]. The thermal energy generated at the friction surfaces is stored in the disc brake through heat conduction. Subsequently, this heat is conducted to the surrounding components of the brake system. However, these surrounding components, such as the wheel cylinders, brake fluid, and wheel bearings, are constrained by the maximum allowable temperature to maintain optimal working conditions. Therefore, the heat stored in the disc must be dissipated as quickly as possible [13]. The primary method for dissipating heat from the discs is through convection, which occurs in two ways: Along the sides of the disc and through the cooling fins. The convective terms are defined as the following general formula [33].

$$Q = Ah(T_d - T_\infty) \tag{26}$$

where, Q is the rate of heat transfer out of the disc (W), h is heat transfer coefficient ($W.m^{-2}K^{-1}$), A is the surface area (m^2), T_d is the surface temperature of the disc (°C), and T_∞ is the temperature of the environment (°C).

Eq. (26) reveals that with an increase in the surface area, the heat transfer out of the disc also rises. To investigate this further, simulations were conducted to explore the thermal behavior of three discs made of the same material, gray cast iron, but differing in surface area (A): Specifically, $A_S < A_{V42} < A_{V32}$. According to the theoretical analysis, it's expected that the disc brake's temperature will decrease as the surface area increases, i.e., T(solid) > T(ventilated disc with 42 fins) > T(ventilated disc with 32 fins). However, an interesting observation arises from Figure 9. In the initial second, the rate of surface temperature increase is identical across all three types of brake discs.

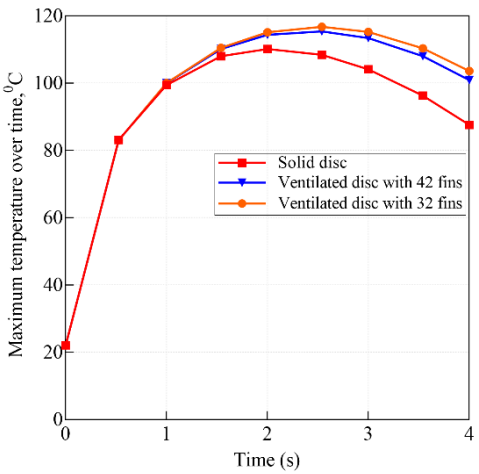

Figure 9. The evolution of maximum temperature over time for variants of grey cast iron discs

Initially, the maximum temperature increases on the surface of the three disc types is similar for about the first second. Subsequently, the maximum temperature of the ventilated disc brake exceeds that of the solid disc over time, i.e., T(solid) < T(ventilated disc with 42 fins) < T(ventilated disc with 32 fins). As shown in Table 1, the mass of the solid disc is greater than that of the ventilated disc. Therefore, the thermal capacity ($C_T = c_p.m_d$) of the solid disc is higher than that of the ventilated disc. This finding clarifies the earlier observation, indicating that the higher maximum temperature of the ventilated disc compared to the solid disc is due to its lower thermal capacity.

Figures 10-15 illustrate the temperature variation on the surface and through the thickness of a quarter of the disc brake. Utilizing gray cast iron, renowned for its high thermal conductivity (as mentioned in section 4.2), in crafting disc brakes promotes efficient heat conduction toward the interior of the disc. Consequently, the peak temperature reached on the disc's surface remains lower compared to discs made from materials with lower thermal conductivity. Moreover, when employing gray cast iron, the surface temperature of the ventilated disc brake exceeds that of the solid disc brake. This is because ventilated brake discs have reduced thermal capacity, hindering the efficient conduction of heat from the surface to the disc's interior. Conversely, when using other materials with low thermal conductivity coefficients, the maximum surface temperatures of solid and ventilated disc brakes are identical. This phenomenon can be explained by the limited time available for heat conduction, coupled with the material's low thermal conductivity, resulting in the retention of heat near the surface.

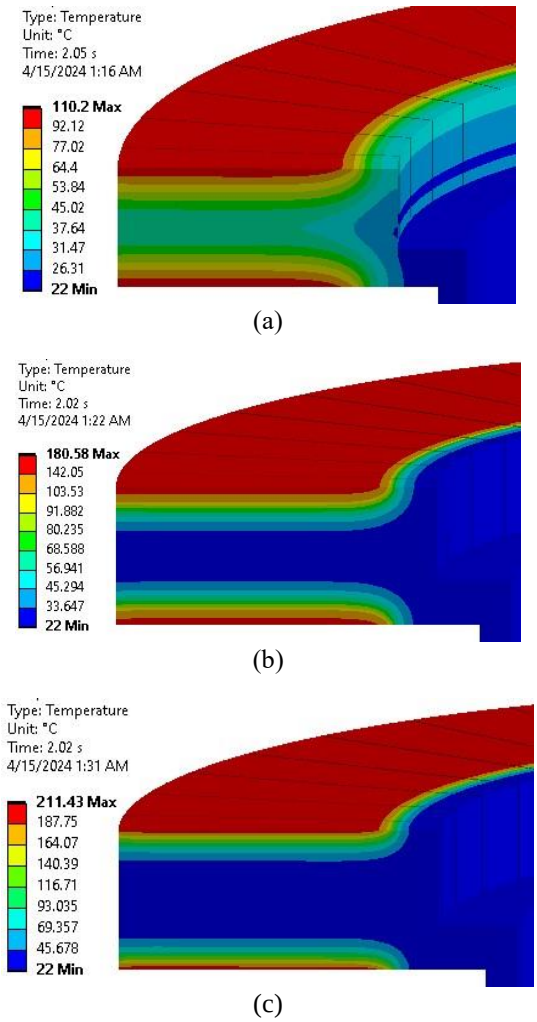

Figure 10. Temperature variation on the surface and through the disc thickness of the solid disc for a material of (a) GCI, (b) AISI 420, and (c) INCONEL 718 when surface reaches the maximum temperature

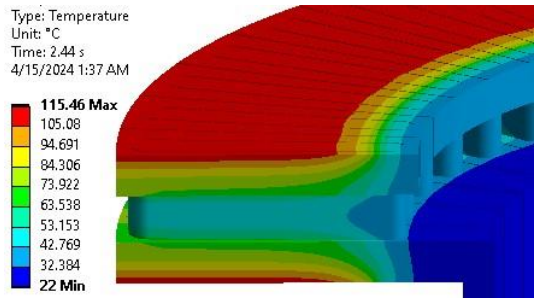

(a)

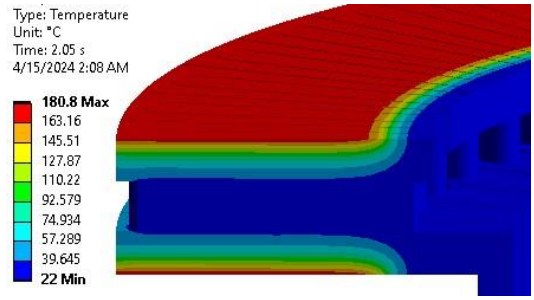

(b)

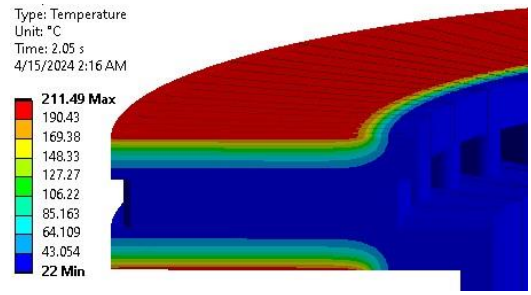

(c)

Figure 11. Temperature variation on the surface and through the disc thickness of the ventilated disc with 42 fins for a material of (a) GCI, (b) AISI 420, and (c) INCONEL 718 when surface reaches the maximum temperature

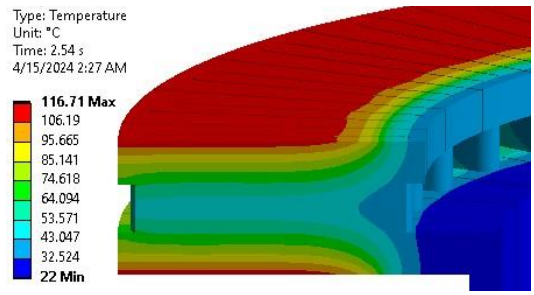

(a)

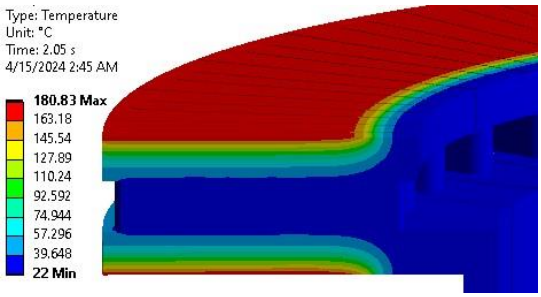

(b)

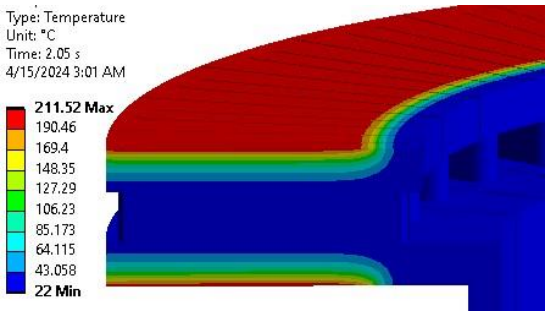

(c)

Figure 12. Temperature variation on the surface and through the disc thickness of the ventilated disc with 32 fins for a material of (a) GCI, (b) AISI 420, and (c) INCONEL 718 when surface reaches the maximum temperature

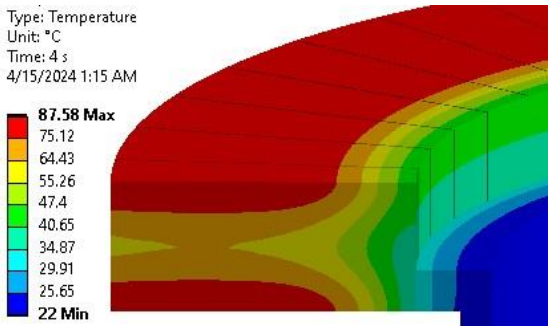

(a)

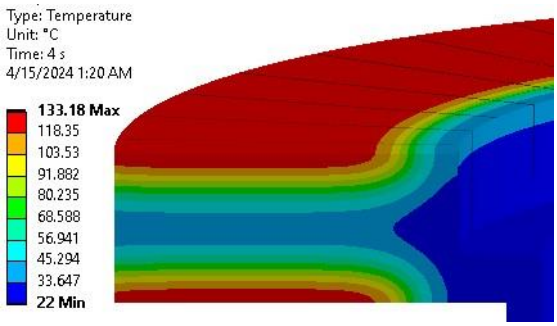

(b)

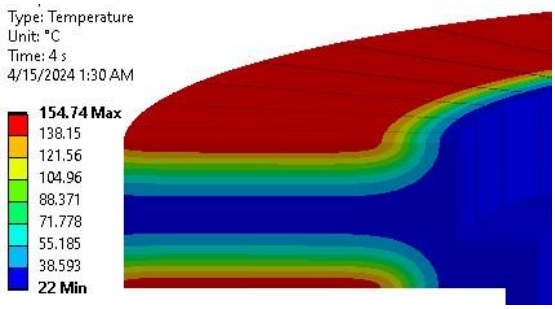

(c)

Figure 13. Temperature variation on the surface and through the disc thickness of the solid disc for a material of (a) GCI, (b) AISI 420, and (c) INCONEL 718 at t = 4s

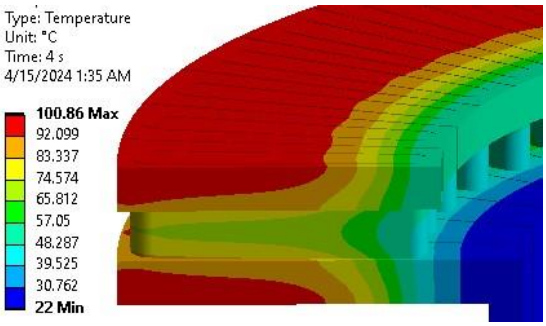

(a)

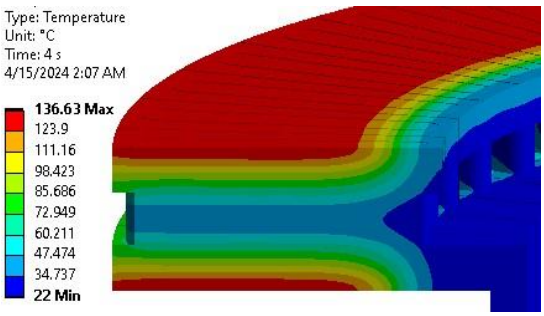

(b)

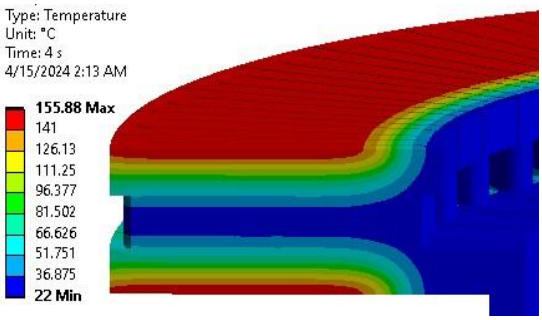

(c)

Figure 14. Temperature variation on the surface and through the disc thickness of the ventilated disc with 42 fins for a material of (a) GCI, (b) AISI 420, and (c) INCONEL 718 at t = 4s

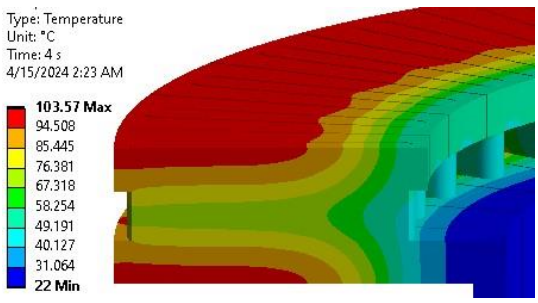

(a)

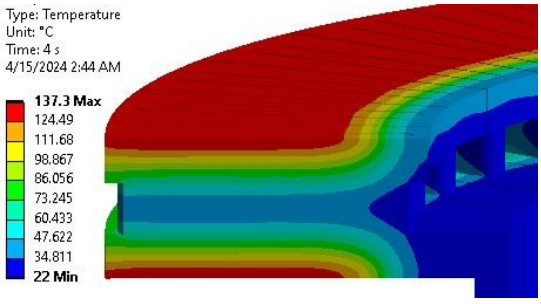

(b)

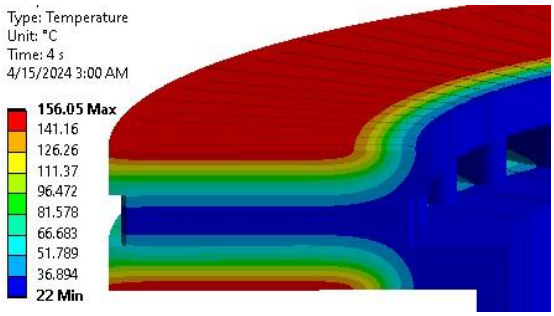

(c)

Figure 15. Temperature variation on the surface and through the disc thickness of the ventilated disc with 32 fins for a material of (a) GCI, (b) AISI 420, and (c) INCONEL 718 at t = 4s

Figure 16 illustrates the temperature distribution of the brake disc at the mean sliding radius and different axial positions. The surface temperature of the brake disc is consistently higher than the internal axial temperature. Notably, this temperature difference decreases towards the end of the braking process for the GCI disc (Figures 16 (b), 16(e), and 16(h)). GCI has higher thermal conductivity than AISI 420 and INCONEL 718 (Table 1). This superior conductivity allows for better heat transfer from the source to the brake disc, leading to a smaller increase in temperature for the same amount of heat. As a result, the surface temperature of the GCI disc is lower than that of the AISI 420 and INCONEL 718 discs. Additionally, Figure 16 shows that for the same material but different configurations, the surface temperature of the solid disc is lower than that of the ventilated disc. This can be explained by the volumetric heat capacity. The volumetric heat capacity ($\rho V c_p$) of the solid disc is higher than that of the ventilated disc. A higher volumetric heat capacity improves heat conduction efficiency, resulting in a smaller increase in surface temperature for the same heat input.

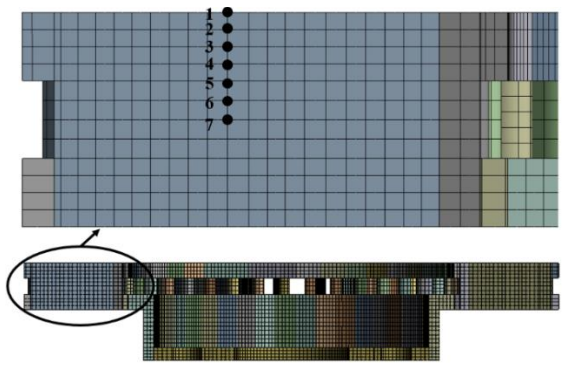

(a) position for temperature measurement on the disc brake

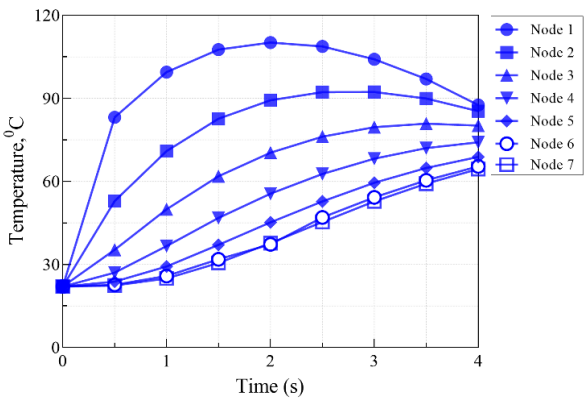

(b) solid disc made of GCI

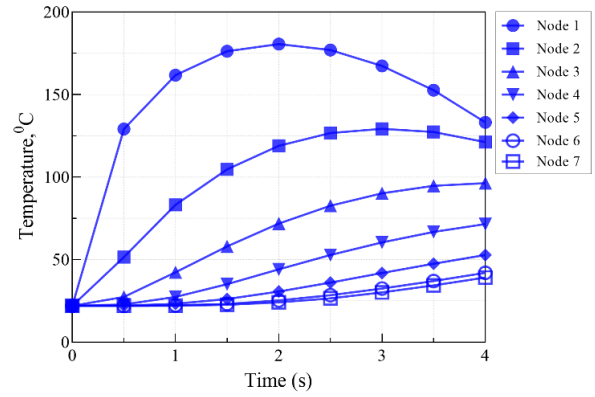

(c) solid disc made of AISIS 420

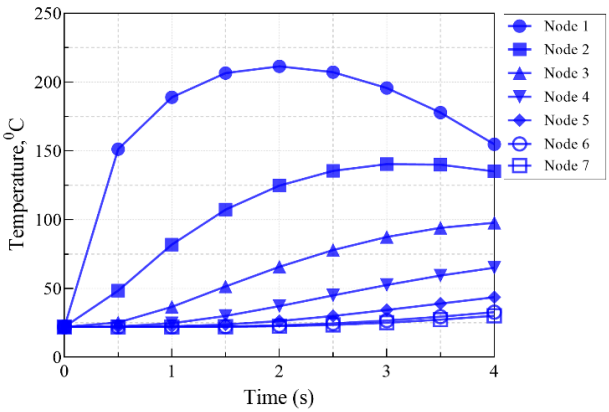

(d) solid disc made of INCONEL 718

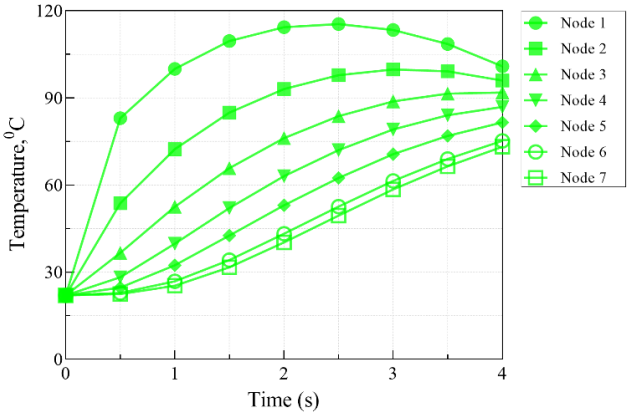

(e) ventilated disc with 42 fins made of GCI

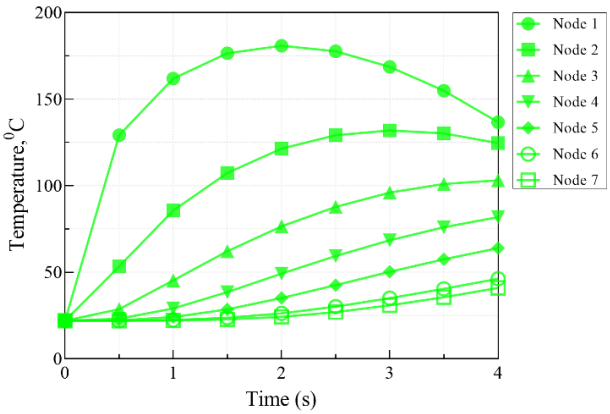

(f) ventilated disc with 42 fins made of AISI 420

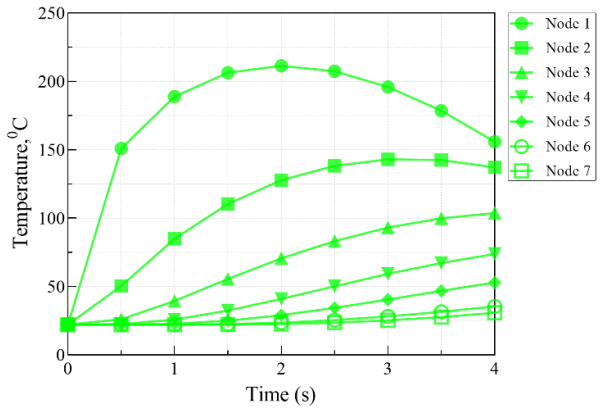

(g) ventilated disc with 42 fins made of INCONEL 718

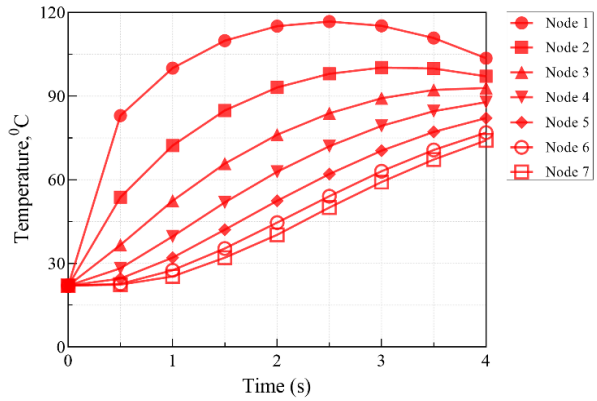

(h) ventilated disc with 32 fins made of GCI

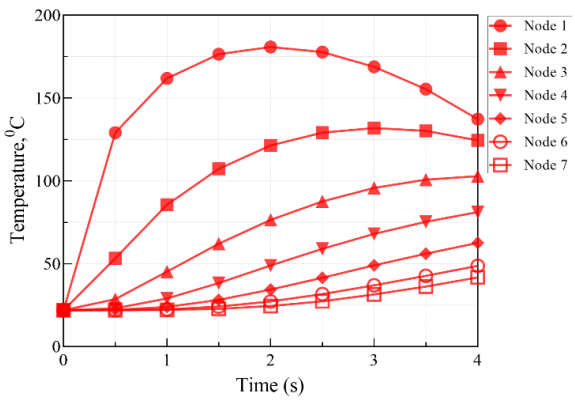

(i) ventilated disc with 32 fins made of AISI 420

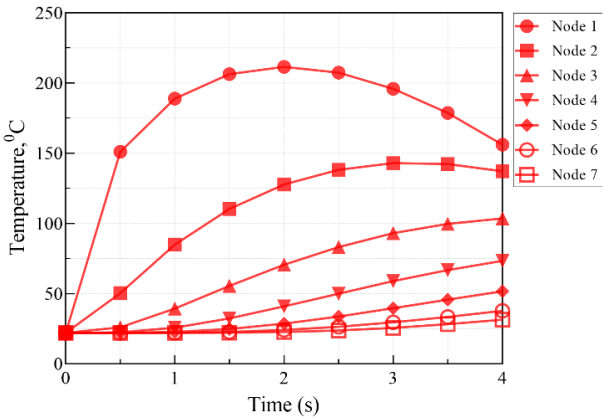

(j) ventilated disc with 32 fins made of INCONEL 718

Figure 16. Temperature variation curves in the axial direction for various materials of three types of brake discs

5. CONCLUSIONS

The study investigated the thermal behavior of solid and ventilated disc brakes during single-stop braking conditions, focusing on three materials: Grey cast iron, AISI 420, and INCONEL 718. The numerical simulations revealed significant differences in thermal performance based on material properties and disc design. Grey cast iron exhibited the lowest maximum temperatures, attributed to its high thermal conductivity, making it a favorable material for brake discs under high thermal loads. Conversely, INCONEL 718, with its lower thermal conductivity, demonstrated the highest maximum temperatures.

Furthermore, the comparison between solid and ventilated discs highlighted the complex interplay between thermal capacity and cooling capabilities. While ventilated discs with 32 and 42 fins showed improved cooling performance, they also exhibited higher maximum surface temperatures compared to solid discs, likely due to their lower thermal capacity. These results emphasize the critical role of material selection and structural design in optimizing brake disc performance, particularly under high thermal stress conditions.

Regarding the future work, we plan to extend this study by exploring the following areas:

1. Investigate the thermal behavior of disc brakes under dynamic braking conditions, including repeated braking events and varying speeds, to better simulate real-world driving scenarios.

2. Evaluate the performance of emerging materials and composites that may offer superior thermal and mechanical properties, potentially improving brake disc performance.

3. Develop and test innovative ventilated disc designs, such as varying fin geometries and incorporating advanced cooling technologies, to optimize heat dissipation.

4. Conduct experimental studies to validate the numerical simulation results and ensure their applicability to practical applications.

ACKNOWLEDGMENT

The authors wish to thank the Thai Nguyen University of Technology for their support.

REFERENCES

[1] Limpert, R. (2011). Brake Design and Safety, Third Edition. SAE International, Warrendale, PA.

[2] Wahlström, J., Olander, L., Olofsson, U. (2010). Size, shape, and elemental composition of airborne wear particles from disc brake materials. Tribology Letters, 38(1): 15-24. https://doi.org/10.1007/s11249-009-9564-x

[3] Nejat, A., Aslani, M., Mirzakhalili, E., Najian Asl, R. (2011). Heat transfer enhancement in ventilated brake disk using double airfoil vanes. Journal of Thermal Science and Engineering Applications, 3(4): 045001. https://doi.org/10.1115/1.4004931

[4] Phan, D., Kondyles, D. (2003). Rotor design and analysis; a technique using computational fluid dynamics (CFD) and heat transfer analysis. SAE Technical Paper 2003-01-3303. https://doi.org/10.4271/2003-01-3303

[5] Yan, H.B., Zhang, Q.C., Lu, T.J. (2016). Heat transfer enhancement by X-type lattice in ventilated brake disc. International Journal of Thermal Sciences, 107: 39-55. https://doi.org/10.1016/j.ijthermalsci.2016.03.026

[6] Wang, L., Lu, X., Li, H., Gong, W., Wang, L. (2022). A new experimental method to study the convective heat transfer characteristics of the interior passages of ventilated disc brakes. International Journal of Thermal Sciences, 179: 107675. https://doi.org/10.1016/j.ijthermalsci.2022.107675

[7] Jafari, R., Erkılıç, K.T., Tekin, O., Akyüz, R., Gürer, M. (2022). Experimental and numerical study of turbulent flow and thermal behavior of automotive brake disc under repetitive braking. Proceedings of the Institution of Mechanical Engineers, Part D: Journal of Automobile Engineering, 236(6): 1092-1100. https://doi.org/10.1177/09544070211040349

[8] Cristol-Bulthé, A.L., Desplanques, Y., Degallaix, G., Berthier, Y. (2008). Mechanical and chemical investigation of the temperature influence on the tribological mechanisms occurring in OMC/cast iron friction contact. Wear, 264(9-10): 815-825. https://doi.org/10.1016/j.wear.2006.12.080

[9] Hui, Y., Liu, G., Zhang, Q., Zhang, Y., Zang, Y., Wang, S., Shi, R. (2023). Fading behavior and wear mechanisms of C/C–SiC brake disc during cyclic braking. Wear, 526-527: 204930. https://doi.org/10.1016/j.wear.2023.204930

[10] Rhee, S.K. (1974). Friction properties of a phenolic resin filled with iron and graphite—sensitivity to load, speed and temperature. Wear, 28(2): 277-281. https://doi.org/10.1016/0043-1648(74)90169-0

[11] Mackin, T.J., Noe, S.C., Ball, K.J., Bedell, B.C., Bim-Merle, D.P., Bingaman, M.C., Bomleny, D.M., Chemlir, G.J., Clayton, D.B., Evans, H.A., Gau, R., Hart, J.L., Karney, J.S., Kiple, B.P., Kaluga, R.C., Kung, P., Law, A.K., Lim, D., Merema, R.C., Miller, B.M., Miller, T.R., Nielson, T.J., O'Shea, T.M., Olson, M.T., Padilla, H.A., Penner, B.W., Penny, C., Peterson, R.P., Polidoro, V.C., Raghu, A., Resor, B.R., Robinson, B.J., Schambach, D., Snyder, B.D., Tom, E., Tschantz, R.R., Walker, B.M., Wasielewski, K.E., Webb, T.R., Wise, S.A., Yang, R.S., Zimmerman, R.S. (2002). Thermal cracking in disc brakes. Engineering Failure Analysis, 9(1): 63-76. https://doi.org/10.1016/S1350-6307(00)00037-6

[12] Duzgun, M. (2012). Investigation of thermo-structural behaviors of different ventilation applications on brake discs. Journal of Mechanical Science and Technology, 26(1): 235-240. https://doi.org/10.1007/s12206-011-0921-y

[13] Limpert, R. (1975). Cooling analysis of disc brake rotors. SAE Technical Paper 751014. https://doi.org/10.4271/751014

[14] Coulibaly, A., Zioui, N., Bentouba, S., Kelouwani, S., Bourouis, M. (2021). Use of thermoelectric generators to harvest energy from motor vehicle brake discs. Case Studies in Thermal Engineering, 28: 101379. https://doi.org/10.1016/j.csite.2021.101379

[15] Jafari, R., Akyüz, R. (2022). Optimization and thermal analysis of radial ventilated brake disc to enhance the cooling performance. Case Studies in Thermal Engineering, 30: 101731. https://doi.org/10.1016/j.csite.2021.101731

[16] Li, C., Yang, H.I. (2023). Optimized shape for improved cooling of ventilated discs. Alexandria Engineering

Journal, 79: 556-567. https://doi.org/10.1016/j.aej.2023.08.035
[17] Gerlici, J., Fomina, Y., Kravchenko, K. (2021). The dependence of the brake disc aerodynamic drag on the rolling stock motion speed. Transportation Research Procedia, 55: 723-730. https://doi.org/10.1016/j.trpro.2021.07.174
[18] Talati, F., Jalalifar, S. (2009). Analysis of heat conduction in a disk brake system. Heat Mass Transfer, 45(8): 1047-1059. https://doi.org/10.1007/s00231-009-0476-y
[19] Majcherczak, D., Dufre´noy, P., Nai¨t-Abdelaziz, M. (2005). Third body influence on thermal friction contact problems: Application to braking. Journal of Tribology, 127(1): 89-95. https://doi.org/10.1115/1.1757490
[20] Yuan, Z.W., Tian, C., Wu, M.L., Zhou, J.J., Chen, C. (2021). Modeling and model validation of thermal behavior of railway disc during single braking. Journal of Thermal Science and Engineering Applications, 13(5): 051017. https://doi.org/10.1115/1.4049984
[21] Yano, M., Murata, M. (1993). Heat flow on disc brakes. SAE Technical Paper 931084. https://doi.org/10.4271/931084
[22] Wahlström, J. (2015). A comparison of measured and simulated friction, wear, and particle emission of disc brakes. Tribology International, 92: 503-511. https://doi.org/10.1016/j.triboint.2015.07.036
[23] Onuike, B., Bandyopadhyay, A. (2018). Additive manufacturing of Inconel 718 - Ti6Al4V bimetallic structures. Additive Manufacturing, 22: 844-851. https://doi.org/10.1016/j.addma.2018.06.025
[24] Athanassiou, N., Olofsson, U., Wahlström, J., Dizdar, S. (2022). Simulation of thermal and mechanical performance of laser cladded disc brake rotors. Proceedings of the Institution of Mechanical Engineers, Part J: Journal of Engineering Tribology, 236(1): 3-14. https://doi.org/10.1177/13506501211009102
[25] Benzley, S.E., Perry, E., Merkley, K., Clark, B., Sjaardama, G. (2011). A comparison of all hexagonal and all tetrahedral finite element meshes for elastic and Elasto-plastic analysis. https://www.semanticscholar.org/paper/A-Comparison-of-All-Hexagonal-and-All-Tetrahedral-Benzley-Perry/dca753a90a12276931e9949d55e814be1d8b5392.
[26] Ray, N., Sokolov, D., Reberol, M., Ledoux, F., Lévy, B. (2017). Hexahedral meshing: Mind the gap. ACM Transactions on Graphics (TOG), 36(4). https://doi.org/10.1145/3072959.2930662
[27] Gao, C.H., Huang, J.M., Lin, X.Z., Tang, X.S. (2007). Stress analysis of thermal fatigue fracture of brake disks based on thermomechanical coupling. Journal of Tribology, 129(3): 536-543. https://doi.org/10.1115/1.2736437
[28] Yang, X., Wang, J.X., Fan, J.C. (2009). Simulation study of temperature field and stress field of disc brake based on direct coupling method. Materials Science Forum, 628-629: 287-292. https://doi.org/10.4028/www.scientific.net/MSF.628-629.287
[29] Maniana, M., Azime, A., Errchiqui, F., Tajmouati, A. (2022). Analytical and numerical analysis of thermal transfer in disc brake. International Journal of Heat and Technology, 40(3): 693-698. https://doi.org/10.18280/ijht.400305
[30] Dubale, H., Paramasivam, V., Gardie, E., Tefera Chekol, E., Selvaraj, S.K. (2021). Numerical investigation of thermo-mechanical properties for disc brake using light commercial vehicle. Materials Today: Proceedings, 46(Part 17): 7548-7555. https://doi.org/10.1016/j.matpr.2021.01.437
[31] Tsai, H.L., Teo, H.G., Gau, C., Jeng, S.T., Lee, C.C., Lin, S.W., Lin, S.C. (2007). Transient thermal analysis of a disk brake system. In Proceeding of the 14th National Computational Fluid Dynamics Conference, New Taipei City, Taiwan.
[32] Cartigny, F., Dufrénoy, P., Desmet, B. (2004). A thermal analysis of a new railway brake concept using liquid cooling. Proceedings of the Institution of Mechanical Engineers, Part F: Journal of Rail and Rapid Transit, 218(2): 79-88. https://doi.org/10.1243/0954409041319605
[33] McPhee, A.D., Johnson, D.A. (2008). Experimental heat transfer and flow analysis of a vented brake rotor. International Journal of Thermal Sciences, 47(4): 458-467. https://doi.org/10.1016/j.ijthermalsci.2007.03.006

NOMENCLATURE

A	Area, m^2
A_S	Area of solid dis, m^2
A_{V32}	Area of ventilated disc with 32 fins, m^2
A_{V42}	Area of ventilated disc with 42 fins, m^2
c_p	Specific heat, $J.kg^{-1}.K^{-1}$
C_T	Thermal capacity, $J.K^{-1}$
$\dot{E}$	Heat rate due to friction, W
$\dot{E}_d$	Heat rate due to friction on disc, W
$\dot{E}_p$	Heat rate due to friction on pad, W
h	Convection heat transfer coefficient, $W.m^{-2}.C^{-1}$
k	Thermal conductivity, $W.m^{-1}.K^{-1}$
m_d	Mass of disc, kg
p	Pressure, $N.m^{-2}$
P_{max}	Maximum pressure, $N.m^{-2}$
q_1	Heat flux on pad, $W.m^{-2}$
q_2	Heat flux on disc, $W.m^{-2}$
r_p	Inner radius in pad, mm
R_p	Outer radius in pad, mm
r_d	Inner radius in disc, mm
R_d	Outer radius in disc, mm
S_p	Pad friction contact surface, m^2
S_d	Disc friction contact surface, m^2
t	Times, s
T_d	Disc brake temperature, ^oC
T_b	Braking time, s
T_0	Initial temperature, ^0K
T_∞	Environment temperature, ^oC

Greek symbols

γ	Heat partition coefficient
μ	Friction coefficient
ξ	Thermal effusivity, $J.m^{-2}.C.s^{0.5}$
ξ_d	Thermal effusivity of disc, $J.m^{-2}.C.s^{0.5}$
ξ_p	Thermal effusivity of pad, $J.m^{-2}.C.s^{0.5}$
ρ	Density, $kg.m^{-3}$
φ_o	Arc angle pad, deg
ω	Wheel speed, $rad.s^{-1}$

ω_o	Wheel initial speed, $rad.s^{-1}$	b	Brake

Subscripts

d	Disc